ORIGINAL PAPER

Rainfall Variability Study in Bangkok and Songkhla Province Thailand using Cross Wavelet Coherence Stationary Oscillation

S. Suwanarat[1, *], S. Chiangga[2], P. Yupapin[3]

[1]Department of Physics, Faculty of Science, Ramkhamheang University, Bangkok 1220, Thailand;
[2]Department of Physics, Faculty of Science, Kasetsart University, Bangkok 1090, Thailand;
[3]Department of Electrical Technology, School of Industrial Technology, Institute of Vocational Education Northeastern Region 2, Sakonnakhon, Thailand

*Corresponding author: *suksanwork@gmail.com*

Received: 04 November 2021 / Revised: 27 December 2021 / Accepted: 29 December 2021

Abstract. Rainfall variability in Southern Asia is strongly affected by local climate, associated with temporal and spatial variations of large-scale atmospheric circulation. Rainfall is a major water source for drinking water and agriculture. For this reason, knowing the interannual relationship between two local climates can provide significant information for forecasting the rainy season to decrease disaster risk and improve water management. In this paper, we present a cross wavelet coherence stationary oscillation (XWCSO) between Arctic- and Antarctic-wide changes in the sea ice extent and rainfall variability at two locations with very different topography, i.e., Bangkok and Songkhla provinces, Thailand. The XWCSO results can be interpreted as large rainfall variability in Bangkok from 1988 to 1990, 2000 to 2007, and 2011 to 2015 during mid-November to mid-March, mid-August to mid-December, and mid-May to mid-September respectively. However, in Songkhla province, the heavy rainfall from 1988 to 2015 occurred from early July until mid-December. Such variability can be connected to the seasonal winds, El Niño and La Niña Southern Oscillation. The proposed scheme should be useful for analyzing and forecasting the rainfall variability over Southeast Asia and other areas, as well as applications in meteorology and agriculture.

Keywords: rainfall variability; stationary oscillation; sea ice extent; cross wavelet coherence

1. Introduction

Rainfall variability is a significant factor affecting the yields of food crops around the world; the variability is directly associated with the influences of the seasonal winds on the topography, as well as the El Niño and La Niña oscillation. This behavior is a non-linear time series in a complex system, in which the periodicities and trends are significant. Wavelet analysis in the non-linear time series is of fundamental interest and has several applications, such as the variability in time series on ice conditions in the Baltic Sea (Jevrejeva et al. 2003; Jevrejeva 2002); the El Niño/Southern Oscillation (ENSO) phenomenon and Indian monsoon rainfall (Narasimha and Bhattacharyya 2010; Torrence and Webster 1999); the southern annular mode driving multi-century wildfire activity in southern South America (Holz et al. 2017); the relationship of the temperature and wind speed data at Adrar, Algeria (Chellali et al. 2010); and analyses of rainfall data (Santos et al. 2003; Yueqing et al. 2004; Rahman et al. 2018; Baddoo et al. 2015; Santos et al. 2001; Cruz et al. 2012; Singh et al. 2020; Sakaros et al. 2021).

Recently, wavelet analysis methods, such as the continuous wavelet transform (CWT), cross wavelet transform (XWT), and wavelet coherence (WTC), have played an important role in examining the relationship between two time series in a time-frequency space that can find localized intermittent periodicities and phase angle statistics, in order to gain confidence in the physical relationships (Jevrejeva et al. 2003; Jevrejeva 2002; Grinsted et al. 2004; Torrence and Compo 1998; Allen and Smith 1996; Daubechies 1990; Fage 1992; Hudgins et al. 1993; Gaucherel 2002). However, this time-frequency space cannot be identified directly with the seasonal time because of the non-stationary element in the time series.

In this paper, the XWCSO is developed to make it applicable for examining the rainfall variability of the rainy season using the obtained stationary

oscillation property of the sea ice extent. Its significant region and phase angles in a time-frequency space stand out in the section of large variability. The sea ice indices, Arctic-wide changes in the Northern Sea ice index (NSIE) and Antarctic-wide changes in the Southern Sea ice index (SSIE) from 1979 to 2015 are calculated on a monthly basis, which presents evidence for differences in variability (based on information maintained by the National Snow and Ice Data Center (NSIDC 2018), University of Colorado, Boulder).

Such indices are significant keys for examining the variability associated with climate systems (NSIDC 2018; Wang and Cai 2013; Carvalho 2005). For example, rainfall data, the Thai Meteorological Department (TMD) has maintained the data from 1979 to 2015 for two regions located in very different topographies (Google 2019). Bangkok is located between a vast land area and the sea in the middle part of Thailand (13°5′N, 100°3′E), and Songkhla province is located between the Gulf of Thailand and the Andaman Sea in the southern part of Thailand (7°2′N, 100°6′E); both are under the influence of the seasonal winds and the intertropical convergence zone (ITCZ) associated with climate change. The XWCSO relationship between the rainfall and the sea ice index is used to find localized intermittent periodicities and phase angle. With the phenomena of the sea ice index, which is stationary oscillation, this relationship can be interpreted as the rainfall variability of the rainy season associated with the topography and the seasonal winds (Santos et al. 2003; Yueqing et al. 2004; Rahman et al. 2018; Baddoo et al. 2015; Santos et al. 2001; Cruz et al. 2012), as well as the El Niño and La Niña oscillation (Jevrejeva et al. 2003; Jevrejeva 2002; Rasmusson and Carpenter 1982; Trenberth 1997; Trenberth and Stepaniak 2011; Trenberth et al. 2019; Huang 1998). The proposed scheme should be useful for analyzing the rainfall variability of the rainy season in Southeast Asia and other areas, as well as for applications in meteorology, agricultural planning, and farming.

2. Theoretical Background

Many signals in nature often display non-stationary oscillations in time series and are generated by complex systems. The XWCSO in the interannual pattern is a relationship between two time series, where one time series is a stationary oscillation and the other one is a non-stationary oscillation. It can be applied to reveal localized intermittent periodicities of seasonal time to link natural mechanisms of the systems. The XWCSO is created by modifying the CWT, XWT, and WTC in order to analyze the interannual relationship as a localized correlation coefficient in a time-frequency space; the Monte Carlo method is employed to assess the statistical significance level against the red noise model, as shown in Formula 1 (see also Jevrejeva 2002; Grinsted et al. 2004; Torrence and Compo 1998; Allen and Smith 1996; Daubechies 1990; Fage 1992; Hudgins et al. 1993; Gaucherel 2002):

$$R_n^2(s) = \left[\frac{\left| [(s^{-1}(W_n^{AB}(s) * c_2 e^{-n^2/2s^2})|_s * c_1 \Pi(0.6s)]|_n \right|^2}{\left| [(s^{-1}(CWT_n^{A}(s) * c_2 e^{-n^2/2s^2})|_s * c_1 \Pi(0.6s)]|_n \right|^2 \left| [(s^{-1}(CWT_n^{B}(s) * c_2 e^{-n^2/2s^2})|_s * c_1 \Pi(0.6s)]|_n \right|^2} \right] \quad (1)$$

Where $W_n^{AB}(s) = CWT_n^{A}(s) \overline{(CWT_n^{B}(s))^*}$ is the XWT between two time series, *A* is the non-linear time series, *B* is the stationary time series, and * denotes the complex conjugate. CWT^A and CWT^B are the continuous wavelet transforms obtained by the Morlet function, c_1 and c_2 are normalization constants, and Π is rectangle function. The factor of 0.6 is the empirically determined scale length for the Morlet wavelet. The common-phase angle is given by

$$\phi_n^{AB}(s) = \tan^{-1}\left(\frac{\mathrm{Im}(W_n^{AB}(s))}{\mathrm{Re}(W_n^{AB}(s))} \right) \quad (2)$$

The CWT of a time series x_n, and $n = 1,\ldots,N$ can achieve a variable resolution in the form of the time frequency space with the uniform time steps Δt given by:

$$\mathrm{CWT}_n^x(s) = \sqrt{\Delta t / s}\sum_{n'=1}^{N} x_{n'}\psi_0\left[(n'-n)\Delta t / s\right] \quad (3)$$

Where the Morlet wavelet function is given by $\psi_0(\eta) = \pi^{-1/4}e^{i\omega_0\eta}e^{(1/2)\eta^2}$ and $\eta = s.\Delta t$ is dimensionless time, the s is wavelet scale, and $\omega = \omega_0 s$ is a non-dimensional frequency ($\omega_0 = 6$).

Many statistical analyses of time series in natural systems are made under the assumption that the probability density function (pdf) is close to normal, at zero (Grinsted et al. 2004). The time series index transformed the pdf that represents evidence for the different variability, where the XWCSO transforms the two-time series into interannual relationships. The high cross coherent power spectrum of a 95% confidence level and the common phase angle are achieved. The time series index transforms the pdf and presents evidence for the difference in variability. The XWCSO transforms the two-time series into the interannual relationships, where the high cross coherent power spectrum of 95% of confidence level is obtained. These results can be interpreted as the correlation in the two-time series between the variability of the system to link-related mechanisms. However, the CWT with the Morlet wavelet function based on the XWCSO does not completely localize in time, so the edge effects cannot be neglected. This effect induces edge artifacts, so it is useful to introduce a Cone of Influence (COI) of the wavelet analysis as the area in the form of the attenuating and discontinuous power spectrum due to the zero padding. The statistical significance of the power spectrum is estimated by using the Monte Carlo method, with a first-order autoregressive (AR1) process against a red noise model (Jevrejeva 2002; Grinsted et al. 2004; Torrence and Compo 1998; Allen and Smith 1996; Daubechies 1990; Fage 1992; Hudgins et al. 1993; Gaucherel 2002).

3. Results and Discussion

The NSIE and SSIE index of the time series from 1979 to 2015 (by maintaining the NSIDC data calculated on a normalized monthly basis) presents evidence for the differences in variability, as shown in Figures 1(a) and 1(b) (top). The positive and negative indices have a higher and lower value than the normal, respectively. The average monthly sea ice extent, in the NSIE and SSIE, both the sea ice extent of the period of six months during mid-November to mid-May and mid-May to mid-November. The maximum and minimum average sea ice extent in the NSIE is 15.34×10^6 km^2 in February and 6.14×10^6 km^2 in September, and the SSIE averages are 18.54×10^6 km^2 in September and 3.09×10^6 km^2 in February. The wavelet power spectra of the NSIE and SSIE are shown in Figures 1(a) and 1(b) (bottom) with the absolute value squared of the wavelet transform. The solid black curve is the 95% confidence level, and the lighter shade, showing the edge effects, is the COI. The spectra show the stationary oscillation or strong periodicity with a 12-month dominant period corresponding to the global wavelet power spectra of 12 months. The period band from the 9th to the 15th months above the 95% (dashed curve) confidence level is shown in Figures 1(a) and 1(b) (right).

The XWCSO between the NSIE and SSIE is the interannual relationship in the high coherent power spectrum and common phase angle relationship, as shown in Figure 2. The observed coherent features in the individual wavelet transform are strong periodicity with the dominant period of 12 months over a long time, and its relative phase angle relationship around the period band during months 9 to 15, with a 95% confidence level, is the strong anti-phase (180°) pointing left. This can be interpreted as the stationary oscillation, where the period does not change over time, in the NSIE and SSIE. In a comparison of the two indices, the phase angle of 360° is a one-year cycle divided into 12 months. Therefore, with the stationary oscillation property and phase angle relationship between the two time series

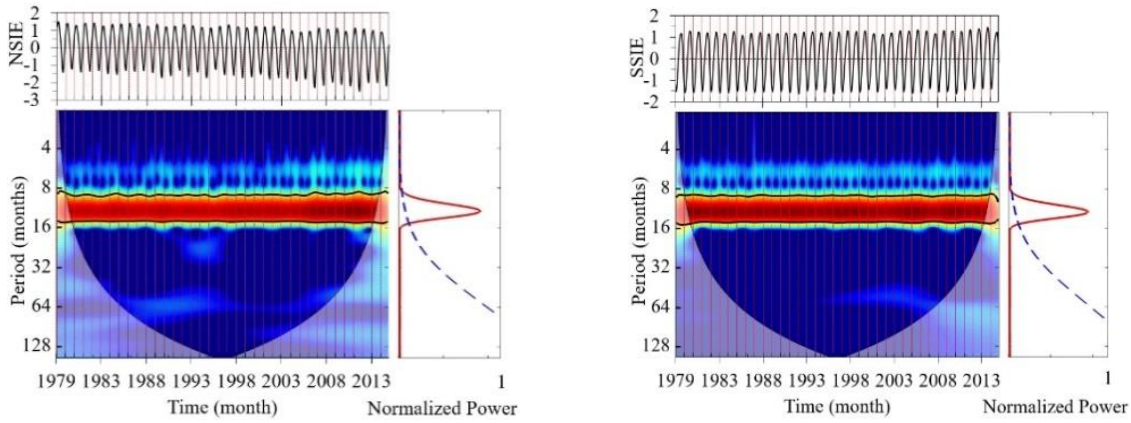

(a) NSIE (b) SSIE

Fig. 1. Normalized time series (top) of (a) the NSIE and (b) the SSIE. Their continuous wavelet power spectra (bottom) have a 95% confidence level against the red noise model within a thick contour and global wavelet power spectrum (right) above the 95% (dashed curve) confidence level.

(under the assumption that the pdf index is normal at zero), it can be useful to link the sea ice season of 12 months running from mid-November until mid-May for the NSIE and from mid-May until mid-November for the SSIE.

In addition, with regard to the XWCSO between the SSIE and NSIE, its spectrum and phase angle relationship are also shown the same period but with the opposite phase angle. Therefore, the sea ice season is similar to the interannual relationship between the NSIE and SSIE, with the NSIE leading the SSIE by six months. By examining the XWCSO, CWT, and the stationary oscillation property of the sea ice index, these can be interpreted as a sea ice season of 12 months, beginning mid-November for the NSIE and mid-May for the SSIE. In addition, the observed period band during the 9th to 15th months (six months) in the CWT is similar to the sea ice extent during mid-November to mid-May for the NSIE and mid-May to mid-November for the SSIE. The wavelet analysis composed of both the XWCSO and CWT can be applied to investigate the seasonal cycle of the time series. By using the stationary oscillation property of the NSIE and SSIE in Earth's natural systems associated with climate change, the XWCSO in the interannual relationship can applied directly to identify the seasonal time in the time series.

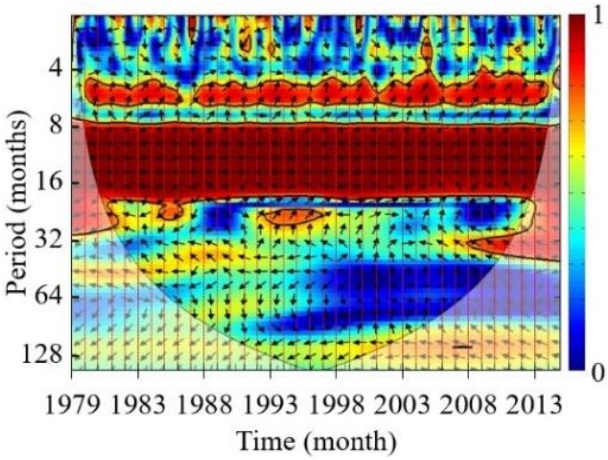

Fig. 2. XWCSO power spectrum and common-phase angle relationship between the NSIE and SSIE with a 95% confidence level against red noise within a thick contour. The phase angle relationship is the strong in-phase of the SSIE leading the NSIE by six months (180°) around the period band of the 9th to 15th months.

In order to examine the rainfall variability that is generated by complex natural systems, the pdf of the monthly rainfall time series is used to analyze the interannual relationship between the rainfall index and the stationary oscillation of the NSIE and SSIE by the XWCSO. Two examples of tropical rainfall data were provided by the Thai Meteorological Department for this study. These locations have two different types of topography; one is located between land and sea in the central part of Thailand – the

capital, Bangkok – and the other is located between the Gulf of Thailand and the Andaman Sea in southern Thailand – Songkhla province – as shown in Figure 3. The interannual relationship of the two regions, both located in a tropical climate zone, is affected by annual monsoons, depressions, typhoons, tropical cyclones, and the ITCZ at different times associated with climate change in each topography, such as land and sea temperatures and atmospheric pressure.

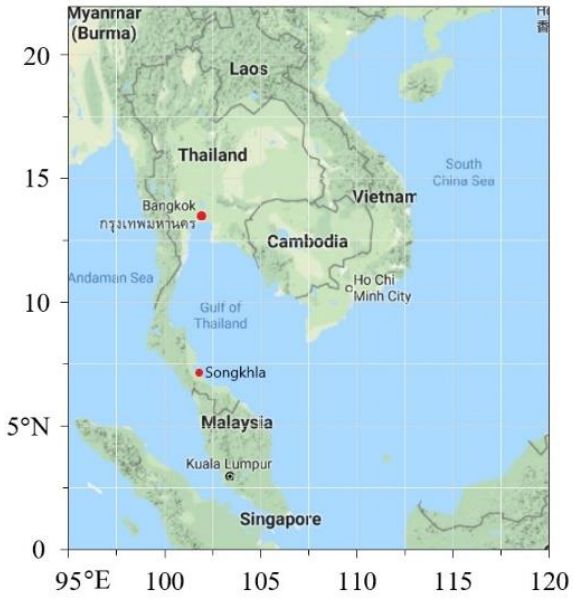

Fig. 3. Locations of the sample sites in Thailand (Bangkok and Songkhla province) for the rainfall data (Google 2019).

Figures 4(a) and 4(b) (top) show the normalized monthly rainfall data from 1979 to 2015 in Bangkok (RBK) and Songkhla province (RSK). The rainfall index is defined by the deviations of the referenced rainfall, in which the positive index is higher than normal, while the negative index is lower than normal. The CWT power spectra of RBK and RSK are shown in Figures 4(a) and 4(b) (bottom); the common feature of the large-scale periodicities of high power within the 95% confidence level is a strong periodicity of 12 months within the period band from 9 to 15 months in RBK, whereas the significant features in the RSK include two strong periodicities of 6 and 12 months within the period band from 5.5 to 7 months and 9 to 15 months, respectively. The global wavelet power spectra in Figures 4(a) and 4(b) (right) with the 95% confidence level (dashed curve) cover the same period. As seen from the spectra, the first cycle of 12 months for both the RBK and RSK is obviously connected to the natural rainy season every year, owing to the seasonal winds, i.e., the southwest and northeast monsoon. The strongest signal regions (with 95% confidence level and which appear along almost the entire spectrum) are related to heavy rainfall. The readings outside the regions are related to little rainfall in the RSK from 1988 to 1991 and in 2006.

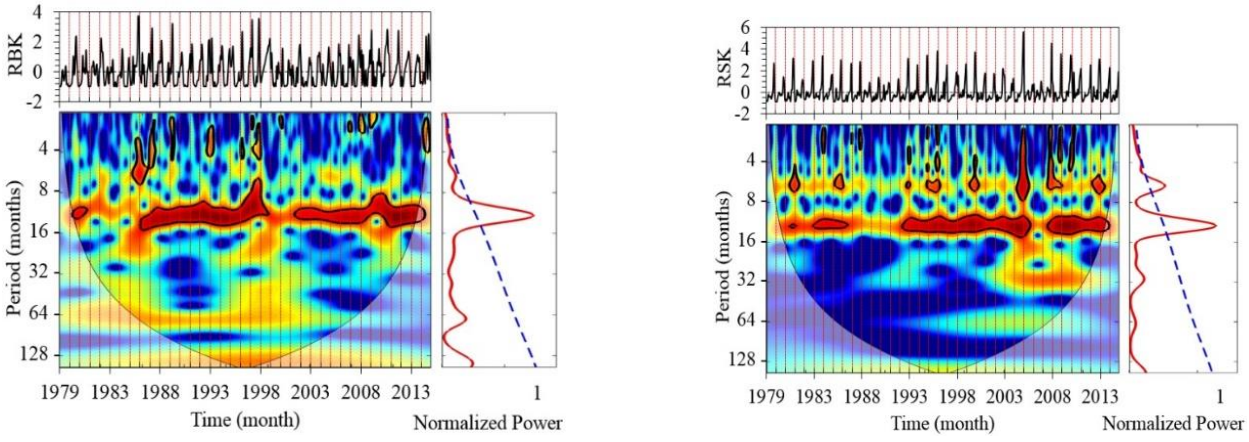

(a) RBK (b) RSK

Fig. 4. Normalized monthly time series (top) of (a) RBK and (b) RSK and their continuous wavelet power spectra (bottom), with a 95% confidence level against a red noise model within a thick contour, and global wavelet power spectra (right) above the 95% (dashed curve) confidence level.

The spectrum in RSK appears also in the second cycle of six months, which has shorter fluctuations that introduce the longer rainy season. In addition, their spectra can identify rain delay and heavy rainfall over a long period. For example, in RSK in 2005, there was heavy rainfall almost all year, which appeared clearly in the power spectra of the period band during months 1 to 12. Likewise, RBK in 1998 had heavy rainfall almost all year and a rain delay, which can be observed in the spectrum increase around one month, with the period band from 1 to 11 months.

The coherence features of the XWCSO power spectrum between the NSIE and RBK in Figure 5(a) clearly show that the rainfall variability of the rainy season in the large region, with a 95% confidence level, is significant within the period band from 9 to 15 months and its dominant period of 12 months over a long period. The relative phase angle relationships, in which RBK leads NSIE, is nearly in-phase (0°), pointing right from 1988 to 1990; the vertical phase (90°) points straight up from 2000 to 2007; and the anti-phase (180°) points left from 2011 to 2015.

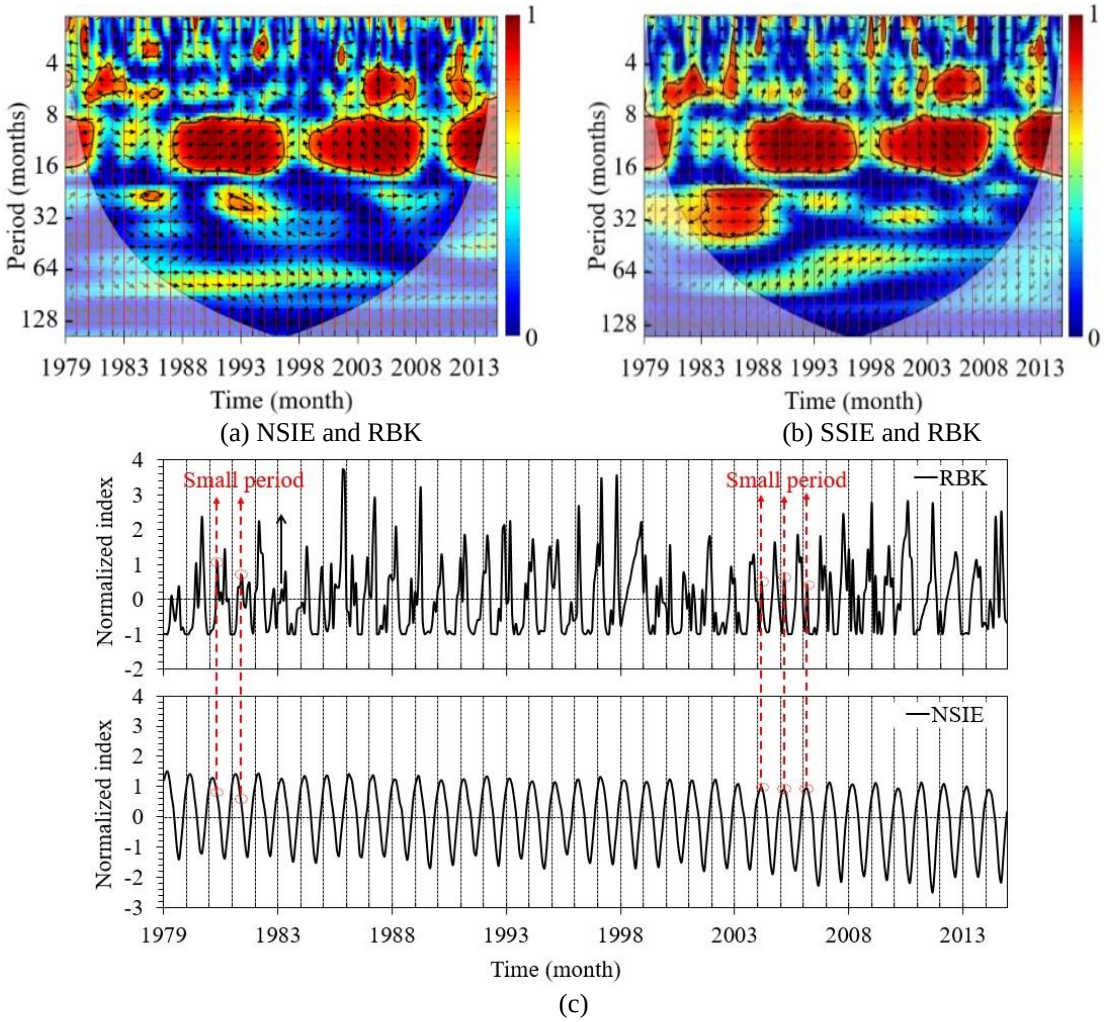

Fig. 5. XWCSO power spectral and phase angle relationship with a 95% confidence level against red noise within a thick contour (a) between the NSIE and RBK; the RBK phase leading the NSIE is nearly in-phase (0°) pointing right from 1988 to 1990, the vertical phase (90°) pointing straight up from 2000 to 2007, and the anti-phase (180°) pointing left from 2011 to 2015; (b) between the SSIE and RBK, with the opposite phase relationship; and (c) the comparative two-time series between the NSIE and RBK.

With the stationary oscillation property of the NSIE and the significant period band of four months in the global wavelet power spectrum of RBK, the XWCSO relationship can be interpreted as rainfall variability from 1988 to 1990, 2000 to 2007, and 2011 to 2015, beginning mid-November (in-phase, RBK leading NSIE is zero month) until mid-March (1988-1990); from mid-August (vertical phase, RBK leading NSIE is three months) until mid-December (2000-2007); and mid-May (anti-phase, RBK leading NSIK is six months) until mid-September (2011-2015). These relationships correspond to the interannual relationship of the NSIE and RBK time series, as shown in Figure 5(c).

Additionally, the XWCSO spectra shows low intensity without 95% confidence in regions associated with the negative index, which points to little rainfall or rain delay, such as from 1981 to 1986, in 1998, and in 2009. The small oscillations appear in the significance period band during 5.5 to 7 months and its dominant period of six months from 1981 to 1983 and 2004 to 2007, where the phase angle relationships are around 150° (4.5 months) and 90° (2.5 months), respectively. These can be interpreted as the rain delay in a short period, around 2.5 months from early April until May and mid-February until mid-April, respectively, corresponding to the interannual relationship of the NSIE and RBK time series in Figure 5(c). However, the interannual relationship between the NSIE and SSIE in Figure 5(b) appears to have the opposite phase angle with the same spectrum. As a result, the rainfall variability of the rainy season can be interpreted as similar to the interannual relationship between the NSIE and SSIE

Figure 6 shows the XWCSO of the interannual relationship between the NSIE and RSK, where its power spectrum, with a 95% confidence level, appears in the two dominant periods of 12 and 6 months. The significant phases obtained by RSK leading the strong phase from NSIE of 135° (4.5 months) and 30° (1 month) occur within the periods of 10 to 14 and 5.5 to 7 months, respectively.

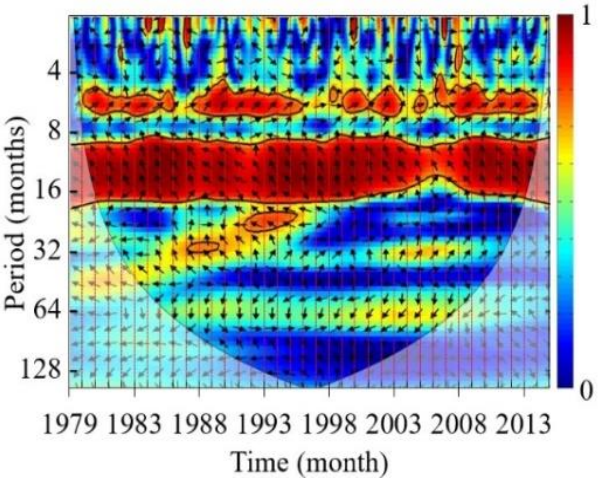

Fig. 6. XWCSO power spectrum and phase angle relationship, with a 95% confidence level, against red noise, within a thick contour between the NSIE and RSK, where the significance phases from RSK lead the strong phase from NSIE.

These can be interpreted as rainfall variability by using the stationary oscillation property of the NSIE and the CWT period band of four months. The natural season cycle of 12 months has the rainfall period of four months (early July until October), and the shorter fluctuations of six months have the rainfall period of 2.5 months (mid-October until mid-December); therefore, in Songkhla province, the rainfall variability occurs in a period of 5.5 months, from early July to mid-December. The XWCSO in an interannual relationship and the stationary oscillation property of the sea ice index has given some insights into the connection between the rainfall variability and the monsoon rainfall in Thailand. Thailand's weather is under the influence of the southwest and northeast monsoon from mid-May to mid-October and mid-October to mid-February, respectively, according to the TMD report. As a result, in Songkhla province, the rainfall variability from 1979 to 2015 during the period from early July to mid-December is affected by both the southwest and northeast monsoon.

Large rainfall variability appears in Bangkok from 1988 to 1990, 2000 to 2007, and 2011 to 2015, during mid-November to mid-March, mid-August to mid-December, and mid-May to mid-September, respectively, affected by the northeast monsoon (1988-1990), the southwest and northeast monsoon (2000-2007), and the southwest monsoon (2011-2015). Similar rainfall variabilities can also connect to an index for the El Niño/Southern Oscillation (ENSO) in the Climate Data Guide, involving the El Niño and La Niña events (Rasmusson and Carpenter 1982; Trenberth 1997; Trenberth and Stepaniak 2011; Trenberth et al. 2019; Huang 1998). The index from 1979 to 2015 revealed a strong El Niño oscillation (El Niño index > 2) in 1983, 1997, and 2015 (Trenberth et al. 2019), which correlates with the anomalous change in the rainfall variability in Bangkok, when there was little rainfall or the rain was delayed. Also, the large rainfall variability from 1988 to 1990, 2000 to 2007, and 2011 to 2015 is related to heavy rainfall associated with the La Niña oscillation. However, the rainfall variability of the rainy season in Songkhla province is almost unaffected by the ENSO.

4. Conclusion

The XWCSO interannual relationship is recognized as a significant tool, which can be used to investigate rainfall variability. The stationary oscillation property of the sea ice extent associated with natural climate change is a significant result that has been obtained through XWCSO. Two sample locations for data on tropical rainfall variability (Bangkok and Songkhla province in Thailand) were examined. The interannual relationship between the NSIE and RBK can be interpreted as large rainfall variability during the rainfall period of four months in Bangkok, which saw heavy rains from 1988 to 1990, 2000 to 2007, and 2011 to 2015, with delayed or shifted rainy seasons. This seasonal time is connected to the raining season and La Niña oscillation and is associated with climate change. Moreover, the anomalous phase changes are related to the low amounts of rainfall in 1983, 1997, and 2015, which can be connected to the strong El Niño oscillation. However, in Songkhla province, the rainfall variability appears strongly significantly in two periods over a long time, which means that it has a natural rainy season of 12 months and a shorter fluctuation of six months. As a result, the rainfall period is 5.5 months during the months of early July to mid-December; it is associated with the seasonal winds, and ENSO has almost no effect on it. The proposed scheme would be useful for investigating the rainfall variability in southern Asia and other areas, as well as applications in meteorology, agricultural planning, and farming.

Acknowledgments

The authors are grateful to the National Snow and Ice Data Center for the sea ice index, the Thai Meteorological Department for the rainfall data, and the Climate Data Guide for El Niño SST indices. The authors also greatly appreciate the support of Institute of Vocational Education Northeastern Region 2, Sakonnakhon, Thailand and the Department of Physics, Faculty of Science, both Kasetsart University and Ramkhamhaeng University, Bangkok, Thailand.

References

Allen MR, Smith LA (1996) Monte Carlo SSA: Detecting irregular oscillations in the presence of coloured noise. J. Clim. 9:3373–3404

Baddoo T, Guan Y, Zhang D, Andam-Akorful S (2015) Rainfall variability in the Huangfuchuang Watershed and its relationship with ENSO. Water **7**(7):3243–3262

Carvalho LMV, Jones C, Ambrizzi T (2005) Opposite phases of the Antarctic oscillation and relationships with intraseasonal to interannual activity in the tropics during the austral summer. J. Clim. 18:702–718

Chellali F, Khellaf A, Belouchrani A (2010) Wavelet spectral analysis of the temperature and wind speed data at Adrar, Algeria. Renewable Energy 35:1214–1219

Cruz FT, Narisma TG, Villafuerte II MQ, Cheng-Chua KU, Olaguera LM (2012) A climatological analysis of the southwest monsoon rainfall in the Philippines. Atmos. Res. 122:609–616

Daubechies I (1990) The wavelet transform time-frequency localization and signal analysis. IEEE Trans. Inform. Theory 36:961–1004

Farge M (1992) Wavelet transforms and their applications to turbulence. Annu. Rev. Fluid Mech. 24:395–457

Gaucherel C (2002) Use of wavelet transform for temporal characterization of remote watersheds. J. Hydrol. 269:101–121

Google (2019) Google Maps. Retrieved September 5, 2019 from http://www.google.co.th/maps/place/ Bangkok/ @11.0641193, 97.7201264,5.31z

Grinsted A, Moore JC, Jevrejeva S (2004) Application of the cross wavelet transform and wavelet coherence to geophysical time series. Nonlin. Processes Geophys. 11:561–566

Holz A, Paritsis J, Mundo IA, Veblen TT, Kitzberger T, Williamson GJ, Araoz E, Bustos-Schindler C, Gonzalez ME, Grau HR, Quezada JM (2017) Southern annular mode drives multicenter wildfire activity in southern South America. Proc. Natl. Acad. Sci. USA. 114(36):9552–9557

Huang J, Higuchi K, Shabbar A (1998) The relationship between the North Atlantic oscillation and the El Niño-southern oscillation. Geophys. Res. Lett. 25:2707–2710

Hudgins L, Friehe CA, Mayer ME (1993) Wavelet transforms and atmospheric turbulence. Phys. Rev. Lett. 71:3279–3282

Jevrejeva S, Moore JC, Grinsted A (2003) Influence of the arctic oscillation and El niño-southern oscillation (ENSO) on ice conditions in the Baltic Sea: the wavelet approach. J. Geophys. Res. 108(D21):4677–4687

Jevrejeva S (2002) Association between the ice conditions in the Baltic Sea and the North Atlantic oscillation. Nordic Hydrol. 33:319–330

National snow and ice data center (2018) Sea ice index: Arctic-and Antarctic-wide changes in sea ice. Available online: https://nsidc.org/data/seaice_index/archives.

Narasimha R, Bhattacharyya S (2010) A wavelet cross-spectral analysis of solar-ENSO-rainfall connec-tions in the Indian monsoons. Appl. Comput. Harmon. Anal. 28:285–295

Rahman R, Anik AM, Farhana Z, Devnath S, Ahmed Z (2018) Pattern recognition of rainfall using wavelet transform in Bangladesh. Open J. Stat. 8:134–145

Rasmusson EM, Carpenter TH, (1982) Variations in tropical sea surface temperature and surface wind fields associated with the southern oscillation/El niño. Mon. Wea. Rev. 110:354–384

Sakaros B, Frédéric F, Gil M, Adrien P, Raphael O, Fabien B, Fernando N, Jacques E, Jean-Jacques B (2021) Investigating links between rainfall variations in the Ogooué River basin and ENSO in the Pacific Ocean over the period 1940–1999. Proc. IAHS, 384: 181–186

Santos CAG, Galvão CO, Suzuki K, Trigo RM (2001) Matsuyama city rainfall data analysis using wavelet transform. J. Hydraul. Engng, JSCE 45:211-216.

Santos CAG, Galvão CO, Trigo RM (2003) Rainfall data analysis using wavelet transform. IAHS-AISH publication, 195–201

Singh A, Thakur S, Adhikary N C (2020) Influence of climatic indices (AMO, PDO, and ENSO) and temperature on rainfall in the Northeast Region of India. SN Appl. Sci. 2: 1728

Torrence C, Compo GP (1998) A practical guide to wavelet analysis. Bull. Am. Meteorol. Soc. 79:61–78

Torrence C, Webster P (1999) Interdecadal changes in the ESNO monsoon system. J. Clim. 12:2679–2690

Trenberth KE (1997) The definition of El niño. Bull. Amer. Meteor. Soc. 78:2771–2777

Trenberth KE, Stepaniak DP (2011) Indices of El niño evolution. J. Clim. 14:1697–1701

Trenberth K, National center for atmospheric research staff (2019) The climate data guide: Nino SST indices (Nino 1+2, 3, 3.4, 4; ONI and TNI), last modified 11 Jan 2019. Available online: https://climatedataguide.ucar.edu/climate-data/nino-sst-indices-nino-12-3-34-4-oni-and-tni

Wang G, Cai W (2013) Climate-change impact on the 20th-century relationship between the southern annular mode and global mean temperature. Sci. Rep. 3:2039

Yueqing X, Shuangcheng L, Yunlong C (2004) Wavelet analysis of rainfall variation in the Hebei Plain. Sci. China Ser. D. 48(12):2241–2250